Quantum optical two-atom thermal diode

Cahit Kargı,[1] M. Tahir Naseem,[1] Tomáš Opatrný,[2] Özgür E. Müstecaplıoğlu,[1,*] and Gershon Kurizki[3]
[1]*Department of Physics, Koç University, 34450 Sariyer, Istanbul, Turkey*
[2]*Department of Optics, Palacký University, 17. listopadu 50, 77146 Olomouc, Czech Republic*
[3]*Department of Chemical and Biological Physics, Weizmann Institute of Science, Rehovot 7610001, Israel*

(Received 30 October 2018; revised manuscript received 23 March 2019; published 16 April 2019)

We put forward a quantum-optical model for a thermal diode based on heat transfer between two thermal baths through a pair of interacting qubits. We find that if the qubits are coupled by a Raman field that induces an anisotropic interaction, heat flow can become nonreciprocal and undergoes rectification even if the baths produce equal dissipation rates of the qubits, and these qubits can be identical, i.e., mutually resonant. The heat flow rectification is explained by four-wave mixing and Raman transitions between dressed states of the interacting qubits and is governed by a global master equation. The anisotropic two-qubit interaction is the key to the operation of this simple quantum thermal diode, whose resonant operation allows for high-efficiency rectification of large heat currents. Effects of spatial overlap of the baths are addressed. We discuss the possible realizations of the model in various platforms, including optomechanical setups, systems of trapped ions, and circuit QED.

DOI: 10.1103/PhysRevE.99.042121

I. INTRODUCTION

A heat diode (HD) is a device that conducts heat under thermal bias in the direction chosen as forward—say, from a heat bath on the left side to a cold bath on the right side of the device—but insulates heat flow under the reverse (backward) thermal bias, i.e., from a hot bath on the right to a cold bath on the left, according to the choice made above [1–4]. The HD proposals and experimental realizations in solid-state [5–10], mesoscopic [11–14], and quantum systems [15–24] attest to the keen interest in this subject, motivated by the expectation that HD would become to phononics [25–30], primarily in the nanoscale and quantum domains, what a semiconducting diode is to micro- or nano-electronics [31–33]. For the realization of these prospects it is essential to acquire a deep understanding of HD operation principles in the quantum domain. Here we set out to resolve the following basic issues of quantum HD operation.

(1) Since HD operation requires reciprocity breaking between forward and backward heat flow at the quantum junction connecting two baths, can we identify a genuine quantum mechanism of such reciprocity breaking? Classically or quasiclassically, an HD junction is commonly viewed as a dissipative ratchet [25,34] where rectification is achieved by the left-right asymmetry (tilt) of its energy spectrum, obstructing the heat flow to the "wrong" side. A ratchet is a spatially extended structure, e.g., a spin chain [35,36], but is there an alternative quantum HD model in the case of a single-atom (dot) junction or a junction comprised of two closely spaced atoms or dots?

(2) A similar question concerns a classical HD mechanism whereby the junction is asymmetrically coupled to the left- and right-heat channels (baths) [37–39] which again requires an extended structure such that the couplings to the two baths are distinct, which may be impossible on nano- or microscales. Can there be an effectively asymmetric coupling to the two baths in the quantum domain, notwithstanding their close proximity or overlap?

(3) Once an HD junction has been constructed, can it be controlled, so as to adapt it to the situation at hand?

In this paper we provide affirmative answers to all three basic questions raised above, by putting forward a simple quantum HD scheme.

First, the proposed scheme is based on two anisotropically interacting qubits. The mechanism responsible for HD operation in this scheme is the left-right asymmetric interaction of the two qubits. It may arise, for example, when an external classical field is aligned with the z axis of the Bloch sphere of one qubit and with the x axis of its counterpart, as proposed by Rao and Kurizki [40]. It is universally adaptable to any material, qubit-level spacing, and temperature and entirely relies on quantum optical tools, i.e., Raman and four-wave mixing transitions that bypass the ratchet (spatial tilt) requirements. Its natural realizations can be found in ferromagnetic systems [41,42] or in nuclear spin environments [43]. It can be engineered, as we shall discuss in Sec. IV, using related model Hamiltonians of various systems such as cavity QED [44–46], trapped ions [47], circuit QED [48–51], and optomechanics [52–55].

Previously, for a junction comprising two interacting qubits, it has been concluded that either the qubits must be off-resonant with each other [24] or that the two baths and the qubit-bath couplings need to have asymmetry, in addition to having different bath temperatures [22–24]. Here we show that neither of the above mechanisms is compulsory for our quantum HD. A system of two anisotropically interacting mutually resonant identical qubits that are symmetrically coupled

*omustecap@ku.edu.tr

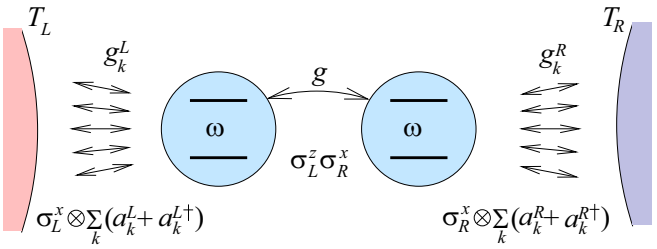

FIG. 1. Schematic diagram of the quantum thermal diode based on two resonant qubits ($\omega_R = \omega_L = \omega$) coupled via anisotropic spin-spin interaction $\sigma_L^z\sigma_R^x$, the coupling strength between the qubits being g. Each qubit is coupled to a single thermal bath, the qubit bath coupling rates being identical. We assume these two baths are independent and may have distinct non-negative temperatures.

to two identical baths (that differ only in temperature) may allow for high-efficiency heat rectification and much higher heat flow than previously suggested schemes.

Second, our analysis elucidates the requirements that the left and right baths be distinct, so that they can be assigned different temperatures and allow for heat flow from one bath to the other, even in case of close proximity or overlap of the baths. Such a scenario requires an analysis based on a global master equation for the entire setup, as previously stressed [56–59] rather than on (generally inadequate) local master equations for each of the qubits [60,61].

Finally, an important aspect of our proposed scheme is its controllability through tuning the strength of the two-qubit Raman-coupling field, which can in turn strongly inhibit or permit four-wave mixing and Raman transitions between the system levels via thermal quanta. Thus, the control Raman field acts as the valve that obstructs or enables global heat transport through the junction.

The paper is organized as follows. In Sec. II we describe our model and discuss the physical mechanism behind the diode operation. In Sec. III we present its results for the heat currents and the rectification factors. We discuss possible implementations of this model scheme in Sec. IV. Finally, we conclude in Sec. V.

II. MODEL AND PHYSICAL MECHANISM

We consider a system of two interacting qubits, with transition frequencies $\omega_{\rm L}$ and $\omega_{\rm R}$ as shown in Fig. 1. The Hamiltonian of the system is (we take $\hbar = 1$)

$$\hat{H} = \frac{\omega_{\rm L}}{2}\hat{\sigma}_{\rm L}^z + \frac{\omega_{\rm R}}{2}\hat{\sigma}_{\rm R}^z + g\hat{\sigma}_{\rm L}^z\hat{\sigma}_{\rm R}^x, \tag{1}$$

where g is the coupling strength of the Raman-induced anisotropic exchange interaction between the left (L) and right (R) qubits and $\hat{\sigma}_\alpha^\beta$ with $\alpha = {\rm L}, {\rm R}$, and $\beta = z, x$ are the Pauli matrices.

In order to derive the global Markovian master equation, we first diagonalize the coupled-qubit system Hamiltonian by a unitary transformation (see Appendix A) that yields the dressed-system Hamiltonian in the form

$$\hat{\tilde{H}} = \frac{\omega_{\rm L}}{2}\hat{\tilde{\sigma}}_{\rm L}^z + \frac{\Omega}{2}\hat{\tilde{\sigma}}_{\rm R}^z, \tag{2}$$

where $\Omega = \sqrt{\omega_{\rm R}^2 + 4g^2}$. The transformed Pauli matrices $\hat{\tilde{\sigma}}_\alpha^\beta$ are given by

$$\hat{\tilde{\sigma}}_{\rm L}^z = \sigma_{\rm L}^z, \tag{3}$$

$$\hat{\tilde{\sigma}}_{\rm R}^z = \cos\theta\hat{\sigma}_{\rm R}^z + \sin\theta\hat{\sigma}_{\rm L}^z\hat{\sigma}_{\rm R}^x. \tag{4}$$

The master equation is derived in Appendix A. In the interaction picture it has the form

$$\dot{\hat{\rho}} = \hat{\mathcal{L}}_{\rm LL} + \hat{\mathcal{L}}_{\rm RR}, \tag{5}$$

where $\hat{\mathcal{L}}_{\rm LL}$ and $\hat{\mathcal{L}}_{\rm RR}$ are Liouville superoperators that describe energy exchange of the system with the baths, whose spectral response functions are given in Appendix A. In the derivation of Eq. (5), we have assumed that the baths are independent and each bath is physically connected with its corresponding qubit. Since this can be difficult to implement in cases of proximity between the qubits, we discuss in Appendix C the case where each bath is physically connected with both qubits.

Although Eq. (5) appears to describe two disconnected L and R subsystems it, in fact, allows for excitation exchange between these subsystems, as required for a heat diode (HD) (see Appendix D). The structure of the dissipators in Eqs. (A16) and (A17) allows us to identify a simple heat valve mechanism in the heat transport; $\hat{\mathcal{L}}_{\rm RR}$ as well as the first two terms in $\hat{\mathcal{L}}_{\rm LL}$ represent the local heat transport channels that couple the baths with the corresponding dressed states $|i\rangle$ of the qubits but do not contribute to HD operation. The last four terms in Eq. (A17) describe the heat transport through the global channels between the two baths, which are the only channels that matter for HD. The different channels are characterized by frequencies ω_{ij} in Fig. 2 with $i, j = 1, 2, 3, 4$; $\omega_{13} = \omega_{24} = \omega_{\rm L}$, $\omega_{14} = \omega_{\rm L} + \Omega$, $\omega_{23} = \omega_L - \Omega$, and $\omega_{12} = \omega_{34} = \Omega$. The channel with spectral response function at frequency $\pm\omega_{23} = \pm(\omega_{\rm L} - \Omega)$ transfers the heat via single-excitation exchange (flip-flop) through the qubits, while the one at frequency $\pm\omega_{14} = \pm(\omega_{\rm L} + \Omega)$ transfers the heat via a two-quanta (Raman) process. In order to open one or both of the global heat transfer channels, which are the only ones that contribute to HD operation, the temperature of the left bath $T_{\rm L}$ needs to be sufficiently high. As the transition $|4\rangle \to |1\rangle$ requires high-energy quanta, $T_{\rm L}$ may not be sufficient to transfer heat by this two-quanta process. As a result, the corresponding channel may be completely or partially obstructed for large g. Therefore, when $T_{\rm L} > \omega_{\rm L} + \Omega > T_{\rm R}$ heat flows from left to right through both local and global channels, but for $T_{\rm R} > T_{\rm L}$ the double excitation channel is obstructed and the heat flow decreases.

The rectification effect can be explained by considering possible cycles between the four states $|1\rangle, |2\rangle, |3\rangle, |4\rangle$ which transmit heat from the hot to the cold bath. In principle, there are three possible Raman cycles (3213), (4214), (4234), and their inverses [here (3213) means the sequence of transitions $|3\rangle \to |2\rangle \to |1\rangle \to |3\rangle$, etc.]. In addition, three four-wave mixing cycles (41234), (43124), (41324), and their inverses are also possible. Among the four-wave mixing cycles, only the cycle (41234) transfers heat between the baths, while the remaining two keep the bath energies unchanged. The transition rate is dependent on the coupling strengths [see

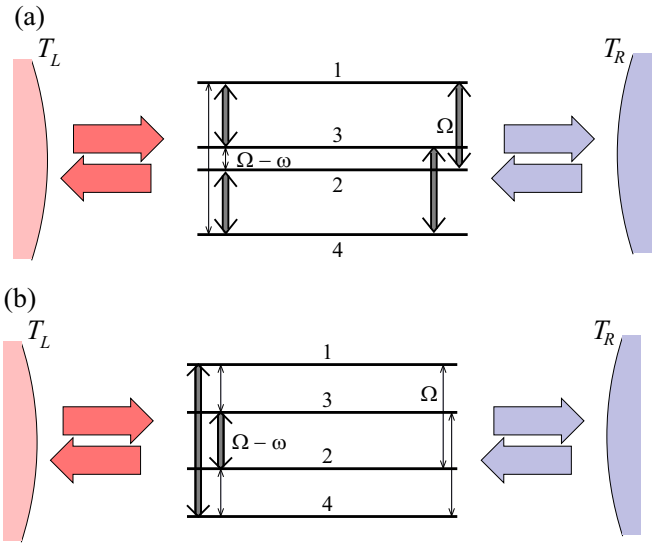

FIG. 2. Same system as in Fig. 1 with Hamiltonian represented by a diagonalized form. The left bath induces transitions $1 \leftrightarrow 3$, $2 \leftrightarrow 3$, $1 \leftrightarrow 4$ and $2 \leftrightarrow 4$, whereas the right bath induces transitions $1 \leftrightarrow 2$ and $3 \leftrightarrow 4$. (a) Small coupling $g \ll \omega$ and (b) large coupling $g = \omega$. The relative strength of the coupling of individual levels induced by the reservoir fields is indicated by the width of the arrows connecting the levels.

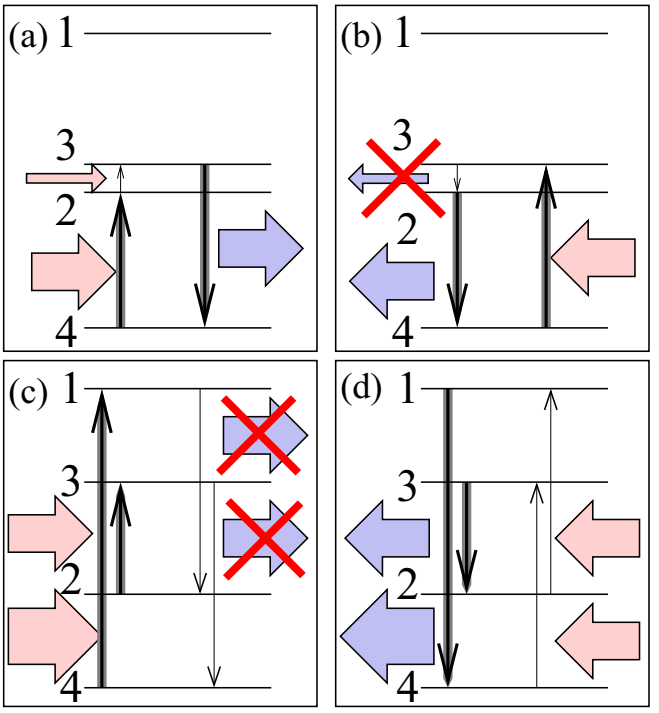

FIG. 3. Examples of processes that rectify heat current with resonant qubits. Panels (a) and (b) correspond to the case with small $g \ll \omega$, and panels (c) and (d) to $g = \omega$. The left column corresponds to heat transfer from left to right, and the right column vice versa. In the case with small g the weakest transition is $|3\rangle \leftrightarrow |2\rangle$ (the strength of the coupling is indicated by the width of the arrows pointing from one level to another). This transition can be induced by a strong field of a hot left reservoir (a). If the left reservoir is cold (b), this transition is inhibited so the system rectifies from left to right. For large g one of the mostly pronounced asymmetries occurs in the four-wave mixing cycle. The coupling is relatively strong on transitions $|2\rangle \leftrightarrow |3\rangle$ and $|1\rangle \leftrightarrow |4\rangle$ and weak on transitions $|1\rangle \leftrightarrow |2\rangle$ and $|3\rangle \leftrightarrow |4\rangle$. Therefore, cycle (41234) carrying heat from left to right (c) is inhibited since the field of the cold right reservoir is not sufficient to induce the weak transitions $|1\rangle \to |2\rangle$ and $|3\rangle \to |4\rangle$. The inverse cycle (43214) can run faster if the weakly coupled transitions are induced by the strong field of the right reservoir (d), so in this regime the system rectifies from right to left.

Eqs. (A16) and (A17)] whose relative magnitudes depend on the mixing angle θ as in Eq. (A2). If some of the coupling strengths between the dressed levels are much smaller than other, they cause a bottleneck in the cycle, and the cycle can be completed only if a sufficiently strong field induces the transition. Thus, the cycle can preferentially run in the direction in which the bottleneck transition is coupled to the hot bath. For resonant qubits ($\omega_L = \omega_R \equiv \omega$) the situation is shown in Figs. 2 and 3 where the coupling strengths are indicated by the widths of the arrows connecting the levels. For weak coupling, $g \ll \omega$, the bottleneck transition in the Raman cycle (4234) is $|2\rangle \leftrightarrow |3\rangle$, which is induced by the left bath [see Fig. 2(a) and Figs. 3(a) and 3(b)] so that the system rectifies heat from left to right. On the other hand, for strong coupling, $g = \omega$, the bottleneck transitions in the four-wave mixing cycle (41234) are $|1\rangle \leftrightarrow |2\rangle$ and $|3\rangle \leftrightarrow |4\rangle$ [see Fig. 2(b) and Figs. 3(c) and 3(d)]. In this case the system rectifies heat from right to left. Similar considerations can be applied to off-resonant qubits (see Appendix B).

The proposed mechanism of the nonreciprocal heat transport relies neither on the frequency difference of the qubits nor on the asymmetry of the dissipation rates of the baths. In our model high rectification can be obtained for resonant qubits with symmetric (identical) couplings to their baths, in contrast to other diode models that rely on asymmetric qubit-bath couplings and difference in qubit frequencies to attain rectification [23,24]. The absence of asymmetry allows us to have two resonant coupled qubits. In contrast to HDs based on off-resonant qubits, resonant qubits endow with unique capabilities of either blocking or conducting a larger heat currents with higher rectification factors than other schemes [23,24], without a trade-off between rectification and heat currents. From the point of view implementation, compact, two-qubit thermal diodes find considerable rectification values for large heat currents even in the case of overlapping baths, thus allowing highly compact designs of HDs. Accordingly, the application significance and the fundamental scheme we consider is radically different from earlier proposals [23,24].

III. HEAT CURRENTS AND RECTIFICATION FACTOR

In order to characterize the heat flow in our system, we calculate the heat currents $\mathcal{J}_R$ and $\mathcal{J}_L$ from the two baths. According to the definition [62] we have

$$\mathcal{J}_R = \mathrm{Tr}[\hat{\mathcal{L}}_{RR}\hat{\tilde{H}}]. \tag{6}$$

The first law of thermodynamics requires that at steady state the heat currents satisfy $\mathcal{J}_R = -\mathcal{J}_L$ (a positive value of the heat current indicates heat flowing from the bath into the

system). Here we report only $\mathcal{J}_R$, and the relation for $\mathcal{J}_L$ is given in Appendix D. Using Eq. (5) in Eq. (6) the heat current from the right bath is

$$\mathcal{J}_R = -\tfrac{1}{2}\kappa_R \Omega \cos^2\theta \big[1 + (2\bar{n}_R + 1) \times \left(\cos\theta\langle\hat{\sigma}_R^z\rangle + \sin\theta\langle\hat{\sigma}_L^z\hat{\sigma}_R^x\rangle\right)\big]. \quad (7)$$

Out of the heat currents one can calculate the rectification factor [3],

$$\mathcal{R} = \frac{|\mathcal{J}_R(T_R, T_L) + \mathcal{J}_R(T_L, T_R)|}{\mathrm{Max}[|\mathcal{J}_R(T_R, T_L)|, |\mathcal{J}_R(T_L, T_R)|]}, \quad (8)$$

where the $\mathcal{J}_R(T_R, T_L)$ is the heat current from the right bath into the system for $T_R > T_L$, and vice versa for $\mathcal{J}_R(T_L, T_R)$ and $T_L > T_R$.

The rectification factor is a figure of merit that measures the quality of the diode, taking values between 0 (symmetric heat flow) and 1 (perfect diode). In our numerical calculations we consider resonant (RQ, $\omega_L = \omega_R$) and off-resonant (ORQ, $\omega_L \neq \omega_R$) qubits for both Ohmic (OSD) and flat (FSD) spectral densities of the baths. The simulations are done using scientific python packages along with key libraries from QuTiP [63].

A. Effects of asymmetric interaction strength

With ORQs, unit rectification is possible for wide range of system parameters. However, here we consider the resonant case to show that unit rectification is also possible for RQs. Note that in the thermal diode models proposed in Refs. [22–24], rectification is not possible for RQs when each qubit is connected to a separate thermal bath.

In Fig. 4 we plot the heat current $\mathcal{J}_R$ and the rectification factor $\mathcal{R}$ for different values of T_L and T_R with RQs and baths with FSD. As can be seen, the heat flow is asymmetric with respect to the $T_L = T_R$ axis [Figs. 4(a) and 4(b)]: For $T_R > T_L$, the heat current $|\mathcal{J}_R|$ is smaller compared to the case when thermal bias is reversed so that the system rectifies heat from left to right. Although rectification is stronger for ORQs, RQs allow the crucial advantage of much larger heat flows; thus, the heat current for RQs is two orders of magnitude larger than for ORQs with $\omega_L = 20\omega_R$, all other parameters being the same.

In Ref. [24] it has been shown that there exists a trade-off between the heat flow and the rectification factor for their model: higher heat currents correspond to lower rectification factors and vice versa. In our case such a trade-off does not exist. To emphasize this point, the heat currents and associated rectification factors are presented in Fig. 5. It is clear from the figure that the higher heat currents are associated with higher rectification factors for both resonant [Figs. 5(a) and 5(c)] and off-resonant [Figs. 5(b) and 5(d)] qubits.

Rectification as a function of interqubit coupling strength g for different values of temperature gradients $\Delta T = T_L - T_R$ is shown in Fig. 6, assuming heat baths with FSD. The rectification shows a nonmonotonic behavior for both off-resonant [Fig. 6(a)] and resonant [Fig. 6(b)] qubits. In both cases rectification decreases with the increase in coupling strength g and it reaches zero, and a further increase in coupling strength results in the increase of rectification. In the ultrastrong coupling regime, the rectification again decreases and becomes zero for $g \gg \omega_L$. This comes about because heat currents vanish in the ultrastrong coupling regime due to the fact that the de-excitation rate from state $|i\rangle$ to state $|j\rangle$ becomes

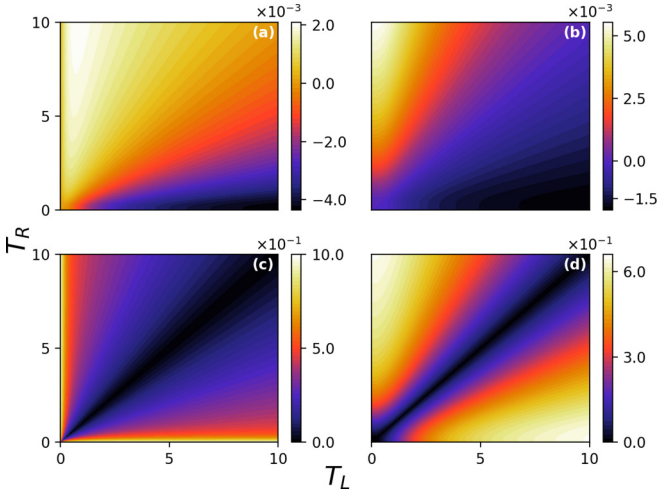

FIG. 4. Steady-state heat current $\mathcal{J}_R$ and rectification $\mathcal{R}$ as functions of temperatures T_L and T_R, assuming heat baths with FSD. Panels (a) and (b) show $\mathcal{J}_R$, and panels (c) and (d) show the corresponding values of $\mathcal{R}$. Almost perfect diode behavior for $g = 0.01$ is obtained only with a large temperature difference $|T_R - T_L|$ as shown in panel (c), and 60% rectification is possible over wide range of bath temperatures if coupling strength is increased to $g = 1$ as shown in panel (d). The interaction strength is $g = 0.01$ in the left and $g = 1$ in the right column. The qubits are resonant with $\omega_L = \omega_R = 1$, and the dissipation rates are $\kappa_{LL} = \kappa_{RR} = 0.01$. All system parameters are scaled with left qubit frequency $\omega_L/2\pi = 10$ GHz.

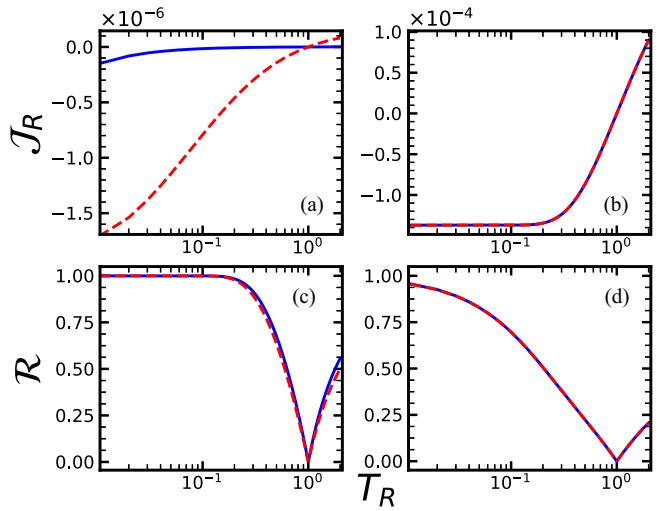

FIG. 5. Steady-state heat current $\mathcal{J}_R$ and rectification $\mathcal{R}$ as functions of temperature T_R, assuming heat baths with FSD. The blue solid curve is for $g = 10^{-4}$, and the red dashed curve is for $g = 10^{-2}$. In the left column qubits are off-resonant; $\omega_L = 1$, $\omega_R = 0.01$, and for the right column they are resonant; $\omega_L = \omega_R = 1$. Panels (a) and (b) show $\mathcal{J}_R$, and panels (c) and (d) show the corresponding values of $\mathcal{R}$. The dissipation rates $\kappa_{LL} = \kappa_{RR} = 0.001$, and left bath temperature $T_L = 1$ is the same in all panels. All system parameters are scaled with left qubit frequency $\omega_L/2\pi = 10$ GHz.

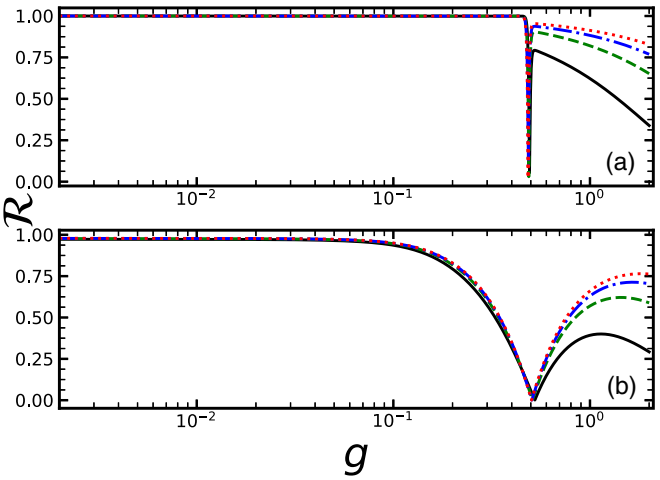

FIG. 6. Rectification $\mathcal{R}$ as a function of coupling strength g, assuming heat baths with FSD. The temperature gradients $\Delta T = T_{\rm L} - T_{\rm R} = 2, 5, 8, 11$ are for black solid, green dashed, blue dashed-dot, and red dotted curves, respectively. One of the baths has fixed temperature 0.01 in ΔT. In the upper panel the qubits are off-resonant, $\omega_{\rm L} = 1$, $\omega_{\rm R} = 0.01$, and for the lower panel they are resonant, $\omega_{\rm L} = \omega_{\rm R} = 1$. The dissipation rates $\kappa_{\rm LL} = \kappa_{\rm RR} = 0.01$ are the same in both panels. All system parameters are scaled with left qubit frequency $\omega_{\rm L}/2\pi = 10$ GHz.

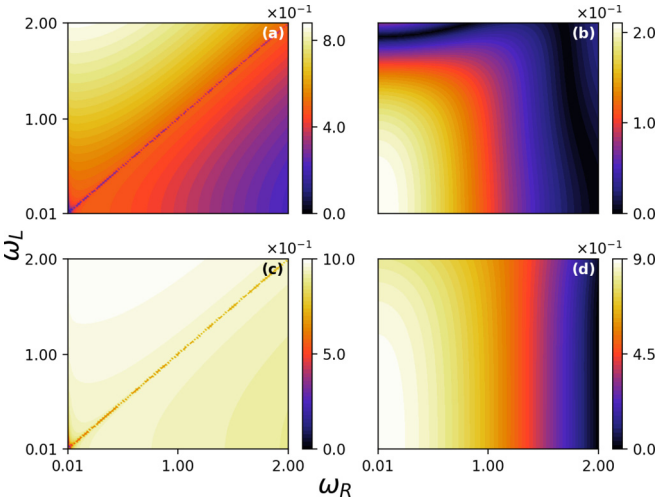

FIG. 7. Rectification $\mathcal{R}$ as a function of the qubit frequencies $\omega_{\rm L}$ and $\omega_{\rm R}$. The interaction strength is $g = 0.5$ in the left and $g = 1$ in the right column. In panels (a) and (b) $T_{\rm R} = 0.5T_{\rm L} = 1$, and in panels (c) and (d) $T_{\rm R} = 0.05T_{\rm L} = 10$. The remaining parameters are the same as in Fig. 4.

equal to the excitation rate from $|j\rangle$ to $|i\rangle$, resulting in a zero transition rate. The two nonzero rectification regimes in Fig. 6 around zero rectification are related to different kinds of processes that transmit heat from the hot to cold bath via global channels. In the weak coupling regime, rectification emerges due to the asymmetry in the Raman processes [Figs. 3(a) and 3(b)] that results in rectification from left to right. In contrast, the rectification in the strong-coupling regime is associated with the four-wave mixing cycles [Figs. 3(c) and 3(d)] that yield right-to-left rectification of heat flow. Since the Raman processes have higher rates than the four-wave mixing counterparts (for the same parameters), the Raman effect is stronger, and therefore the rectification in the weak-coupling regime is higher than in the strong-coupling regime (as shown in Fig. 6). Between these two regimes, there is a dip in the rectification that corresponds to the value of g at which $\omega_{\rm L} - \Omega \approx 0$. This dip appears because at this value of g the energy levels 2 and 3 become degenerate, and the structural asymmetry of the energy levels vanishes, so that rectification becomes zero. This physical interpretation of Fig. 6 is valid only if the colder-bath temperature is very low; $T_\alpha < 0.01$. For higher temperatures of the colder bath, the qualitative behavior of rectification becomes more complex and difficult to interpret.

The nonmonotonic behavior of rectification presented in Fig. 6 is not unique to our model; similar trends have been reported in the case of two interacting qubits coupled asymmetrically with three independent thermal baths [23]. One important difference between the two models is that for resonant qubits, in the model of Ref. [23], rectification varies slightly with the coupling strength g and vanishes for symmetric bath couplings. By contrast in our model, not only do we observe a change in the rectification direction but also obtain nonzero rectification for symmetric bath couplings. It is clear from Fig. 6 that higher rectifications can be achieved for a higher temperature gradient ΔT.

Our calculations show similar properties for baths with OSD. However, the temperature domain of high rectification is then larger, while the heat current is reduced compared to the baths with FSD. This is related to the asymmetry of the spectrum and the proportionality of the spectral response functions to the transition frequencies.

B. Variation of qubit parameters

In the previous subsection, we showed that the RQs behave as a thermal diode, whose rectification depends on coupling strength g. Let us now analyze the effect of qubits coupling-strength variation on the rectification. Figure 7 shows $\mathcal{R}$ for two different coupling strengths, $g = 0.01$ in the left column and $g = 1$ in the right column. Figures 7(a) and 7(b) are for a small temperature difference between the two baths, while Figs. 7(c) and 7(d) correspond to large temperature differences. As can be seen, a large temperature difference increases the diode quality irrespective of the strength of the qubit-qubit coupling. However, RQs generate vanishing rectification for a small value of coupling strength $g = 0.01$ as depicted in Fig. 7(c). On the other hand, almost unit rectification of the heat current by RQs can be obtained if the coupling strength is increased to $g = 1$ [Fig. 7(d)]. All these results demonstrate that the diode quality can be controlled in a wide-range variation of the system parameters. For instance, as shown in Fig. 4(c), the RQ model with $g = 0.01$ behaves as a thermal diode for a narrow range of temperatures; however, this range can be extended by changing the qubit frequencies as shown in Fig. 7. System-bath coupling rates can have another control parameter for the rectification, but here we consider them to be symmetric. A brief discussion of the effect of dissipation rates on rectification is presented in Appendix C.

IV. PHYSICAL MODEL SYSTEMS FOR POSSIBLE IMPLEMENTATIONS

Our HDs rely on asymmetric spin-spin interactions, e.g., $\sigma_L^z\sigma_R^x$ such interaction can be found, for example, in magnetic molecules embedded in nuclear spin environments [43] or in weakly ferromagnetic systems with spin-orbit coupling [41,42]. Similar spin bath models have been used to explore controlling dephasing of a single qubit [40]. The interaction $(\sigma_L^z\sigma_R^x)$ has also been proposed in Ref. [52] for its similarity to optomechanical coupling. Here we provide more details on the realization of such interactions.

A. Optomechanical route for $\sigma_L^z\sigma_R^x$

The optomechanical coupling between an optical resonator of frequency ω and a mechanical resonator of frequency Ω can be written as [53,54]

$$H = \omega a^\dagger a + \Omega b^\dagger b + g a^\dagger a(b + b^\dagger), \tag{9}$$

where the annihilation and creation operators of photons and phonons are denoted by $a, a^\dagger$ and $b, b^\dagger$, respectively. A statistical mutation of bosonic operators to spin operators can be constructed as an inversion of spin to boson Holstein-Primakoff transformation [64]

$$a^\dagger a = J\mathbb{1} + J_z, \quad a = \frac{1}{\sqrt{J\mathbb{1} + J_z}} J_-,$$
$$a^\dagger = J_+ \frac{1}{\sqrt{J\mathbb{1} + J_z}}, \tag{10}$$

where J is the total spin and $J_\pm, J_z$ satisfy the SU(2) algebra. Applying this transformation to both photons and phonons, and assuming weakly excited spins ($\langle J_z\rangle \ll J$), the bosonic optomechanical model can be mapped to the asymmetric spin-spin coupling model. Replacing a bosonic mechanical mode by a single spin-1/2 is justified by assuming $\langle b^\dagger b\rangle \ll 1$, so that only the two lowest vibronic levels are accessible [55].

The weak excitation condition as well as the absence physical qubits make the optomechanical route a limited and indirect approach to implement our HD scheme. The other restrictions, such as weak g or the frequency difference of optical and mechanical modes, can be relaxed in electrical analogs of optomechanical couplings [48].

B. Coupled Raman model route for $\sigma_L^z\sigma_R^x$

The Hamiltonian of a system consisting of a three-level atom in a single-mode cavity is given by

$$H = \omega a^\dagger a + \omega_r |r\rangle\langle r| + \omega_e |e\rangle\langle e| + \omega_g |g\rangle\langle g|$$
$$+ g(a^\dagger(|g\rangle\langle r| + |e\rangle\langle r|) + \text{H.c.}, \tag{11}$$

where g is the cavity-atom coupling coefficient, and $\omega_r, \omega_e, \omega_g$ denote the upper, middle, and lowest energy levels with the associated states $|r\rangle, |e\rangle, |g\rangle$, respectively. Assuming the lower doublet of energy levels are quasidegenerate ($\omega_e \approx \omega_g$) and taking the detuning $\delta = \omega_r - \omega_e - \omega_a$ of the cavity mode from the atomic resonance as much greater than g, then the upper level can be adiabatically eliminated from the dynamics, which can be described by an effective Hamiltonian of the form

$$H = \omega_c a^\dagger a + \epsilon\sigma_z - \frac{g^2}{\delta} a^\dagger a \sigma_x. \tag{12}$$

This two-photon transition model is known as the Raman coupled model [44,46]. Here the intensity-dependent Stark shift in the cavity frequency is neglected; we introduced $\epsilon = \omega_e - \omega_g$, and $\sigma_z = |e\rangle\langle e| - |g\rangle\langle g|$, $\sigma_x = |e\rangle\langle g| + |g\rangle\langle e|$. Similarly to the optomechanical case, one can assume weak excitation of the cavity mode and replace $a^\dagger a$ with σ_L^z to get the desired asymmetric spin-spin interaction.

The Raman route is quite generic provided that we assume only two vibronic levels are involved in an optical Raman scattering from a molecule. The Raman scattering of a field E is described by the interaction $q|E|^2$ where q is the vibrational displacement which can be replaced by σ_x in the case of two-level approximation for the vibrational motion. Using $E \sim (a + a^\dagger)$ and neglecting two-photon terms, $a^\dagger a\sigma_x$ is obtained [45].

C. Quantum walk with trapped ions scheme for $\sigma_L^z\sigma_R^x$

The quantum walk on a circle can be simulated by trapped ions where the steps of the walker are taken in quantum optical phase space according to the single step generator [47]

$$U = \mathrm{e}^{ip\sigma_z} H, \tag{13}$$

where p is the momentum operator generating the step conditioned by the result of the coin toss operation. Here H stands for the Hadamard gate operator. It is proposed that the step can be implemented using four Raman beam pulses sequentially [47]. Assuming the vibrational excitation is much less than 1, the effective Hamiltonian associated with the step generator corresponds to the asymmetric spin-spin interaction $\sigma_L^z\sigma_R^x$.

D. Circuit QED scheme for $\sigma_L^z\sigma_R^x$

A general Hamiltonian of a superconducting resonator interacting with a superconducting qubit can be expressed as [49]

$$H = \omega a^\dagger a + \frac{\Omega}{2} + g(\cos\theta\sigma_z + \sin\theta\sigma_x)(a + a^\dagger), \tag{14}$$

where ω is the frequency of the resonator with the annihilation and creation operators a and $a^\dagger$, respectively. The qubit frequency is denoted by Ω. The coupling coefficient g and the mixing angle θ depend on Josephson-Junction properties. By adjusting the junction parameters to data in $\theta = 0$ one gets the so called phase-gate term [50], which becomes $\sigma_L^z\sigma_R^x$ if the resonator is weakly excited.

E. Two-qubit Raman coupled scheme for $\sigma_L^z\sigma_R^x$

So far we have considered effective qubit systems to implement $\sigma_L^z\sigma_R^x$ coupling. Let us now assume a pair of three-level atoms, each held separately in two bimodal optical cavities. The cavities are coupled to each other via single-mode fibers as depicted in Fig. 8. This scheme is a generalization of the one for single-mode cavities described in Ref. [51]. We consider the general case where the atomic transitions are driven by both classical laser and cavity fields. The interaction

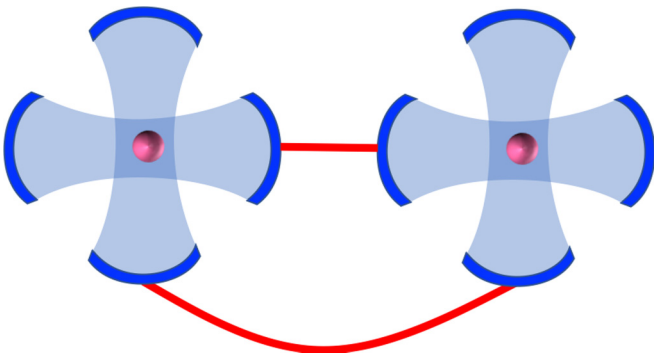

FIG. 8. Schematic diagram of two distant three-level atoms trapped inside fiber coupled bimodal cavities.

picture Hamiltonian describing the coupling of atoms and lasers is

$$H_1 = \sum_{k=L,R} \sum_{x=e,g} \Omega_{kx} e^{i\Delta_{kx}t} |r_k\rangle\langle x_k| + \text{H.c.}, \tag{15}$$

where Ω_{kx} is the Rabi frequency associated with the transition $|r_k\rangle \leftrightarrow |x_k\rangle$ and Δ_{kx} denotes the detuning of the laser from the respective transition. Similarly, the interactions of the cavity modes and the atoms are expressed in the interaction picture as

$$H_2 = \sum_{k=L,R} \sum_{x=e,g} g_{kx} a_{kx} e^{i\delta_x t} |r_k\rangle\langle x_k| + \text{H.c.} \tag{16}$$

Here a_{kx} and $a_{kx}^\dagger$ are the annihilation and creation operators for the respective cavity modes and δ_x is the cavity detuning from the respective transition. The cavities are assumed to be connected through single-mode (short) fibers. The optical interactions are described by the Hamiltonian

$$H_3 = \sum_{e,g} \nu_x b_x (a_{Lx}^\dagger + a_{Rx}^\dagger) + \text{H.c.}, \tag{17}$$

where g_{kx} is the atom-cavity coupling coefficient, and ν_x is the coupling strength of the fiber mode and the respective cavity mode. Creation and annihilation operators for the fiber modes are denoted by b_x and $b_x^\dagger$, respectively. The notation is shown in Fig. 9 for clarity. These Hamiltonians are generalizations of those in Ref. [51]. The only new ingredient here is that we allow for an additional classical drive and a cavity field acting on each atom, such that each transition can be driven by both classical and cavity fields.

The full Raman-coupled model allows us to engineer a variety of qubit-qubit interactions, including asymmetric ones. In particular we can assume that in one transition, e.g., $|r_L\rangle \leftrightarrow |g_L\rangle$, it is driven by the classical and cavity fields, while in the second qubit, a classical field drives the $|r_R\rangle \leftrightarrow |g_R\rangle$ transition and the cavity field drives the $|r_R\rangle \leftrightarrow |e_R\rangle$ transition (Fig. 9). This scheme would yield an effective qubit-qubit coupling $|e_L\rangle\langle e_L| \otimes |g_R\rangle\langle e_R|$ that depends on the population of the $|e_L\rangle$. Taking into account the Hermitian conjugate process we get the $\sigma_{\rm L}^z \sigma_{\rm R}^x$ interaction.

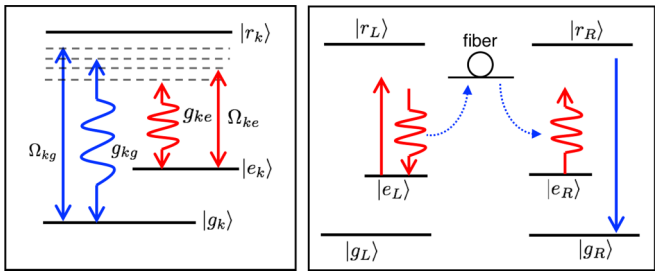

FIG. 9. (Left panel) The classical laser and cavity-field–driven transitions in the three-level atoms, distinguished by label $x = L, R$ for the atom trapped in the left or right cavity (cf. Fig. 8). Both the classical and cavity fields drive the transitions. Upper, middle, and lower atomic states are denoted by $|r_x\rangle$, $|e_x\rangle$, and $g_x\rangle$, respectively. (Right panel) Special case where only the $|r_L\rangle \leftrightarrow |e_L\rangle$ is driven by both the classical laser and the cavity field. The other fields on the left atom are turned off. The right atom is driven by a single classical and a single cavity field in the Raman configuration.

V. CONCLUSION

We have investigated a quantum thermal diode composed of two qubits coupled via anisotropic exchange interaction. By deriving the global master equation, analytical expressions for the heat currents in the system have been found. We have used the rectification factor to quantify the diode quality, calculating the results for both flat and Ohmic spectral densities of the thermal baths. The rectification mechanism is explained in terms of the anisotropic exchange interactions: the baths can excite only some of the transitions in the Raman or four-wave-mixing global cycles so that some global cycles can run only in one direction and not oppositely. We have shown that in our model the diode behavior relies neither on the asymmetry of qubit frequencies nor on the difference of dissipation rates of the heat baths. Rectification can be achieved even for resonant qubits, thus allowing it to conduct large heat currents without compromising rectification efficiency. Since the anisotropic exchange model can be applied to natural weak ferromagnets [41,42], nuclear spin environments [40,43], cavity QED [44–46], circuit QED [48–51], trapped ions [47], and optomechanical systems [48,52,55], we anticipate that our results can be significant for heat management in such systems.

ACKNOWLEDGMENTS

Ö.E.M. acknowledges fruitful discussions with W. Niedenzu and R. Uzdin. C.K. thanks the QUB-CTAMOP and Reykjavik University Nanophysics groups where some of this work was completed for their hospitality. C.K. thanks M. Paternostro, A. Manolescu, and N. Aral for useful discussions. Ö.E.M. and M.T.N. thank O. Pusuluk for pointing out typographical errors. Ö.E.M. and C.K. acknowledge support from the Koç University TÜPRAŞ Energy Center (KUTEM). T.O. acknowledges the support of the Czech Science Foundation (GAČR), grant 17-20479S. G.K. acknowledges the support of DFG, ISF, and SAERI.

APPENDIX A: GLOBAL MASTER EQUATION

We present the derivation of global master equation given in Eq. (5). The system Hamiltonian is diagonalized using the unitary transformation

$$U := \exp\left(-i\frac{\theta}{2}\hat{\sigma}_{\rm L}^{z}\hat{\sigma}_{\rm R}^{y}\right), \tag{A1}$$

where the angle θ is defined as

$$\sin\theta := \frac{2g}{\Omega}, \quad \cos\theta := \frac{\omega_{\rm R}}{\Omega}, \quad \tan\theta := \frac{2g}{\omega_{\rm R}}, \tag{A2}$$

such that $\Omega := \sqrt{\omega_{\rm R}^2 + 4g^2}$. The transformed operators then read

$$\hat{\tilde{\sigma}}_{\rm L}^{x} = U\hat{\sigma}_{\rm L}^{x}U^{\dagger} = \cos\theta\hat{\sigma}_{\rm L}^{x} + \sin\theta\hat{\sigma}_{\rm L}^{y}\hat{\sigma}_{\rm R}^{y}, \tag{A3}$$

$$\hat{\tilde{\sigma}}_{\rm L}^{y} = U\hat{\sigma}_{\rm L}^{y}U^{\dagger} = \cos\theta\hat{\sigma}_{\rm L}^{y} - \sin\theta\hat{\sigma}_{\rm L}^{x}\hat{\sigma}_{\rm R}^{y}, \tag{A4}$$

$$\hat{\tilde{\sigma}}_{\rm L}^{z} = U\hat{\sigma}_{\rm L}^{z}U^{\dagger} = \sigma_{\rm L}^{z}, \tag{A5}$$

and

$$\hat{\tilde{\sigma}}_{\rm R}^{x} = U\hat{\sigma}_{\rm R}^{x}U^{\dagger} = \cos\theta\hat{\sigma}_{\rm R}^{x} - \sin\theta\hat{\sigma}_{\rm L}^{z}\hat{\sigma}_{\rm R}^{z}, \tag{A6}$$

$$\hat{\tilde{\sigma}}_{\rm R}^{y} = U\hat{\sigma}_{\rm R}^{y}U^{\dagger} = \sigma_{\rm R}^{y}, \tag{A7}$$

$$\hat{\tilde{\sigma}}_{\rm R}^{z} = U\hat{\sigma}_{\rm R}^{z}U^{\dagger} = \cos\theta\hat{\sigma}_{\rm R}^{z} + \sin\theta\hat{\sigma}_{\rm L}^{z}\hat{\sigma}_{\rm R}^{x}. \tag{A8}$$

The back transformations from dressed operators to bare operators read from Eqs. (A3)–(A8) by switching dressed operators to bare operators and vice versa with θ replaced by $-\theta$. Then, with the transformation Eq. (A1), the Hamiltonian in Eq. (1) is diagonalized to the Hamiltonian given in Eq. (2).

Eigenstates of the dressed Hamiltonian are given by the individual eigenstates of the qubits as

$$|1\rangle = \cos\frac{\theta}{2}|{+}{+}\rangle - \sin\frac{\theta}{2}|{+}{-}\rangle, \tag{A9}$$

$$|2\rangle = \sin\frac{\theta}{2}|{+}{+}\rangle + \cos\frac{\theta}{2}|{+}{-}\rangle, \tag{A10}$$

$$|3\rangle = \cos\frac{\theta}{2}|{-}{+}\rangle + \sin\frac{\theta}{2}|{-}{-}\rangle, \tag{A11}$$

$$|4\rangle = \cos\frac{\theta}{2}|{-}{-}\rangle - \sin\frac{\theta}{2}|{-}{+}\rangle, \tag{A12}$$

with their corresponding eigenvalues $\omega_1 = \frac{1}{2}(\omega_{\rm L} + \Omega)$, $\omega_2 = \frac{1}{2}(\omega_{\rm L} - \Omega)$, $\omega_3 = \frac{1}{2}(-\omega_{\rm L} + \Omega)$, and $\omega_4 = \frac{1}{2}(-\omega_{\rm L} - \Omega)$, respectively.

The qubits are coupled to two baths of temperature $T_{\rm R}$ and $T_{\rm L}$ via the the Hamiltonian $\hat{H}_{SB}^{ij} = \hat{\sigma}_i^{x} \otimes \sum_k g_k^j(\hat{a}_k^j + \hat{a}_k^{j\dagger})$, where g_k^j are the coupling strengths to baths, and $\hat{a}_k^j$ ($\hat{a}_k^{j\dagger}$) are the creation (annihilation) operator of the k mode of the bath i, $j = {\rm L}, {\rm R}$, whose Hamiltonian is $\hat{H}_j = \sum_k \omega_k \hat{a}_k^{j\dagger}\hat{a}_k^j$. To calculate the master equation, we move to the interaction picture in which

$$\begin{aligned}\hat{\sigma}_{\rm L}^{x}(t) = {}& \cos\theta\hat{\tilde{\sigma}}_{\rm L}^{-}e^{-i\omega_{\rm L}t} - \sin\theta\hat{\tilde{\sigma}}_{\rm L}^{+}\hat{\tilde{\sigma}}_{\rm R}^{-}e^{-i(\Omega-\omega_{\rm L})t} \\ & + \sin\theta\hat{\tilde{\sigma}}_{\rm L}^{-}\hat{\tilde{\sigma}}_{\rm R}^{-}e^{-i(\Omega+\omega_{\rm L})t} + {\rm H.c.},\end{aligned} \tag{A13}$$

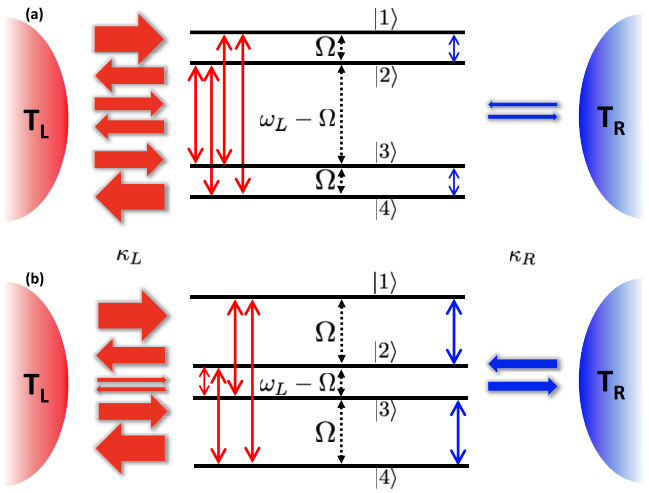

FIG. 10. Same system, but for off-resonant qubits with $\omega_{\rm R} \ll \omega_{\rm L}$, and the system Hamiltonian represented by a diagonalized form. The left bath induces transitions $1 \leftrightarrow 3$, $2 \leftrightarrow 3$, $1 \leftrightarrow 4$ and $2 \leftrightarrow 4$, whereas the right bath induces transitions $1 \leftrightarrow 2$ and $3 \leftrightarrow 4$. (a) Small coupling g and (b) large coupling g for off-resonant qubits. In both cases the left bath is at a higher temperature than the right bath.

$$\hat{\sigma}_{\rm R}^{x}(t) = \cos\theta\hat{\tilde{\sigma}}_{\rm R}^{-}e^{-i\Omega t} + \tfrac{1}{2}\sin\theta\hat{\tilde{\sigma}}_{\rm L}^{z}\hat{\tilde{\sigma}}_{\rm R}^{z} + {\rm H.c.} \tag{A14}$$

Hence, the master equation in the interaction picture is found to be the one that is given in Eq. (5), with

$$G_{ij}(\omega) = \begin{cases}\kappa_{ij}(\omega)[1 + \bar{n}_j(\omega)], & \omega > 0 \\ \kappa_{ij}(|\omega|)\bar{n}_j(|\omega|), & \omega < 0, \\ 0, & \omega = 0\end{cases} \tag{A15}$$

where $\bar{n}_j(\omega) := 1/(\exp\omega/T_j - 1)$ is the average excitation number of $j = {\rm L}, {\rm R}$ baths. We define $\kappa_{ij}(\omega)$ as rates which are independent of frequency for the flat spectrum and $\kappa_{ij}(\omega) = \kappa_{ij}\omega$ for the Ohmic spectrum:

$$\begin{aligned}\hat{\mathcal{L}}_{\rm Lj} = {}& G_{\rm Lj}(\omega_{\rm L})\cos^2\theta\hat{\mathcal{D}}[\hat{\tilde{\sigma}}_{\rm L}^{-}] + G_{\rm Lj}(-\omega_{\rm L})\cos^2\theta\hat{\mathcal{D}}[\hat{\tilde{\sigma}}_{\rm L}^{+}] \\ & + G_{\rm Lj}(\omega_{23})\sin^2\theta\hat{\mathcal{D}}[\hat{\tilde{\sigma}}_{\rm L}^{-}\hat{\tilde{\sigma}}_{\rm R}^{+}] \\ & + G_{\rm Lj}(-\omega_{23})\sin^2\theta\hat{\mathcal{D}}[\hat{\tilde{\sigma}}_{\rm L}^{+}\hat{\tilde{\sigma}}_{\rm R}^{-}] \\ & + G_{\rm Lj}(\omega_{14})\sin^2\theta\hat{\mathcal{D}}[\hat{\tilde{\sigma}}_{\rm L}^{-}\hat{\tilde{\sigma}}_{\rm R}^{-}] \\ & + G_{\rm Lj}(-\omega_{14})\sin^2\theta\hat{\mathcal{D}}[\hat{\tilde{\sigma}}_{\rm L}^{+}\hat{\tilde{\sigma}}_{\rm R}^{+}],\end{aligned} \tag{A16}$$

$$\hat{\mathcal{L}}_{\rm Rj} = G_{\rm Rj}(\Omega)\cos^2\theta\hat{\mathcal{D}}[\hat{\tilde{\sigma}}_{\rm R}^{-}] + G_{\rm Rj}(-\Omega)\cos^2\theta\hat{\mathcal{D}}[\hat{\tilde{\sigma}}_{\rm R}^{+}], \tag{A17}$$

where the first index represents left (L) or right (R) qubit, and the second index $j = {\rm L}, {\rm R}$ is for baths with $\theta = \arctan(2g/\omega_{\rm R})$. In the main text, we consider $\kappa_{ij} = 0$ for distinct i and j. The Lindblad dissipators $\hat{\mathcal{D}}[\hat{A}]$ are defined as [65,66]

$$\hat{\mathcal{D}}[\hat{A}] = \hat{A}\hat{\rho}\hat{A}^{\dagger} - \tfrac{1}{2}(\hat{A}^{\dagger}\hat{A}\hat{\rho} + \hat{\rho}\hat{A}^{\dagger}\hat{A}). \tag{A18}$$

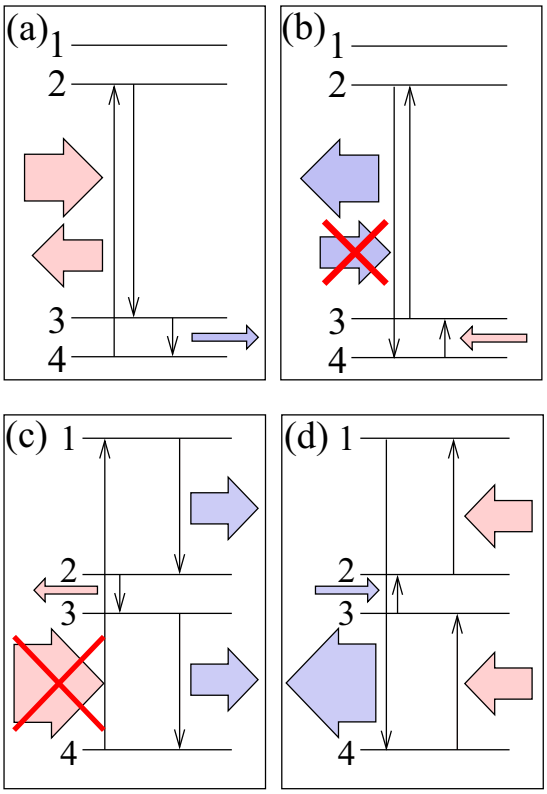

FIG. 11. Examples of processes that rectify heat current for off-resonant qubits, and $\omega_R \ll \omega_L$. Panels (a) and (b) correspond to small g, and panels (c) and (d) to large g; panels (a) and (c) show the left bath is hotter than the right one, and in panels (b) and (d) it is vice versa. For small g, heat can flow from left to right, e.g., via the Raman cycle (4234) (a), whereas the opposite cycle (4324) (b) is inhibited because the cold reservoir cannot excite the $|3\rangle \to |2\rangle$ transition. For large g and for temperatures of the hot reservoir that cannot excite $|4\rangle \to |1\rangle$ transition, the four-wave mixing cycle (41234) (c) may not be achieved, whereas the opposite cycle (43214) (d) can conduct heat from right to left.

APPENDIX B: OFF-RESONANT QUBITS

The different transitions between dressed energy levels with $\omega_R \ll \omega_L$ for the case of off-resonant qubits are shown in Fig. 10(a) for small g and in Fig. 10(b) for large g. The transitions with red arrows are induced by the left bath, and those with blue arrows are induced by the right bath. To explain the rectification in the case of off-resonant qubits, for example, we consider the Raman cycle (4234) for small g as shown in Figs. 11(a) and 11(b). If the left bath is hot, i.e., $T_L > T_R$ [Fig. 11(a)], the cycle may be completed. However, if $T_R > T_L$ [Fig. 11(b)], then the left bath cannot excite the $|3\rangle \to |2\rangle$ transition, and consequently the heat transfer from right to left is inhibited and the device rectifies heat from left to right.

As another example, consider the four-wave mixing cycle (41234) for large g as shown in Figs. 11(c) and 11(d). If the left bath is hot [Fig. 11(c)], but not hot enough to excite the $|4\rangle \to |1\rangle$ transition, the heat transfer from the left to the right bath is inhibited. On the contrary, if the right bath is hot [Fig. 11(d)], the reverse cycle may be completed without obstruction, so that the device rectifies heat from right to left.

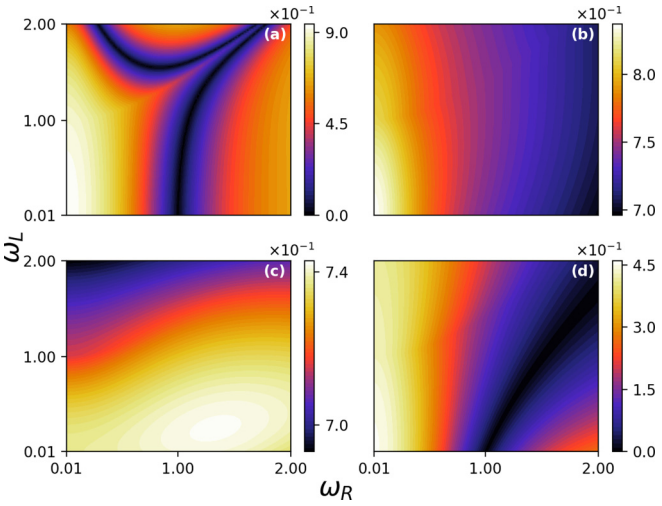

FIG. 12. Rectification $\mathcal{R}$ for the cases with different coupling rates between both baths to both qubits. Panel (a) shows the local bath case. Panels (b) and (c) show the case with both baths accessing their local qubits symmetrically but asymmetrically to the other one. Panel (c) is the case with all qubit-bath couplings symmetric. In all panels, $T_L = 10$, $T_R = 0.5$, and $\kappa_{LL} = \kappa_{RR} = 0.01$. The rest of the parameters are the same as in Fig. 4.

APPENDIX C: CASE OF SPATIALLY OVERLAPPING THERMAL BATHS

In our treatment, we have assumed that each bath is connected only to its corresponding qubit. The assumption of local baths for the qubits, however, is restrictive for possible implementations of our thermal diode scheme. In practice, thermal baths can overlap spatially over the closely spaced pair of interacting qubits. Systems where such an overlap can be absent can still be found. One scenario is to use optomechanical-like coupling of two transmission line resonators as proposed in Ref. [48]. If the resonators are weakly excited in the limit of a single photon, then the system mimics the case of two interacting qubits with local baths realized by thermal noise currents fed into the transmission-line resonators. In other implementations, such as trapped ions [47], off-resonant Raman systems [46], or asymmetric exchange interactions [41,42], spatial overlap of the thermal baths is unavoidable. Apart from such extra design, we would like to now address the question of to what extent can spatial overlap of the baths over the qubit pair be tolerated for a significant thermal rectification? To this end, we consider a generalization of our master equation (5) by including the cross terms $\hat{\mathcal{L}}_{LR}$ and $\hat{\mathcal{L}}_{RL}$, describing the access of the nonlocal thermal baths to both qubits in the bare-state picture. In general, spatial overlap degrades the thermal diode quality by decreasing the maximum rectification factor. On the other hand, in the case of different coupling rates of the baths to their distant qubits we have found that the lowest value of the rectification factor is increased, as shown in Figs. 12(b) and 12(c), compared to Fig. 12(a), which shows the case $\kappa_{LR} = \kappa_{RL} = 0$, which is equivalent to the local case given in

Eq. (5). When the cross-coupling rate is about half of the local coupling rate, then the rectification factor is reduced from ∼90% to ∼45%. When all the coupling rates are equal to each other, the rectification is practically lost.

We conclude that if the spatial overlap of the thermal baths cannot be avoided, then either asymmetric coupling rates to distant qubits should be sought, or, alternatively, additional measures can be taken such that render the baths effectively local [67,68].

APPENDIX D: DYNAMICS AND THE HEAT CURRENTS

Equations of motions for the relevant dynamical observables of our system are determined from the master equation (5) and given by

$$\frac{d}{dt}\langle\hat{\tilde{\sigma}}_{\rm L}^{z}\rangle = \cos^2\theta[G_{\rm L}(-\omega_{\rm L})\langle\mathbb{A}\rangle - G_{\rm L}(\omega_{\rm L})\langle\mathbb{B}\rangle] + \frac{1}{2}\sin^2\theta[G_{\rm L}(\omega_1)\langle\mathbb{A}\mathbb{D}\rangle - G_{\rm L}(-\omega_1)\langle\mathbb{B}\mathbb{C}\rangle + G_{\rm L}(-\omega_2)\langle\mathbb{A}\mathbb{C}\rangle - G_{\rm L}(\omega_2)\langle\mathbb{B}\mathbb{D}\rangle], \tag{D1}$$

$$\frac{d}{dt}\langle\hat{\tilde{\sigma}}_{\rm R}^{z}\rangle = \cos^2\theta[G_{\rm R}(-\Omega)\langle\mathbb{C}\rangle - G_{\rm R}(\Omega)\langle\mathbb{D}\rangle] + \frac{1}{2}\sin^2\theta[-G_{\rm L}(\omega_1)\langle\mathbb{A}\mathbb{D}\rangle + G_{\rm L}(-\omega_1)\langle\mathbb{B}\mathbb{C}\rangle + G_{\rm L}(-\omega_2)\langle\mathbb{A}\mathbb{C}\rangle - G_{\rm L}(\omega_2)\langle\mathbb{B}\mathbb{D}\rangle], \tag{D2}$$

$$\frac{d}{dt}\langle\hat{\tilde{\sigma}}_{\rm L}^{z}\hat{\tilde{\sigma}}_{\rm R}^{z}\rangle = \cos^2\theta\big[G_{\rm L}(-\omega_{\rm L})\langle\mathbb{A}\hat{\tilde{\sigma}}_{\rm R}^{z}\rangle - G_{\rm L}(\omega_{\rm L})\langle\mathbb{B}\hat{\tilde{\sigma}}_{\rm R}^{z}\rangle + G_{\rm R}(-\Omega)\langle\mathbb{D}\hat{\tilde{\sigma}}_{\rm L}^{z}\rangle - G_{\rm R}(\Omega)\langle\mathbb{C}\hat{\tilde{\sigma}}_{\rm L}^{z}\rangle\big], \tag{D3}$$

where we introduce the operators $\mathbb{A} = (\mathbb{1} - \hat{\tilde{\sigma}}_{\rm L}^{z})$, $\mathbb{B} = (\mathbb{1} + \hat{\tilde{\sigma}}_{\rm L}^{z})$, $\mathbb{C} = (\mathbb{1} - \hat{\tilde{\sigma}}_{\rm R}^{z})$, and $\mathbb{D} = (\mathbb{1} + \hat{\tilde{\sigma}}_{\rm R}^{z})$.

The heat currents evaluate to

$$\mathcal{J}_{\rm L} = \tfrac{1}{2}\omega_{\rm L}\cos^2\theta[G_{\rm L}(-\omega_{\rm L})\langle\mathbb{A}\rangle - G_{\rm L}(\omega_{\rm L})\langle\mathbb{B}\rangle] + \tfrac{1}{4}\sin^2\theta[\omega_1 G_{\rm L}(-\omega_1)\langle\mathbb{B}\mathbb{C}\rangle - \omega_1 G_{\rm L}(\omega_1)\langle\mathbb{A}\mathbb{D}\rangle - \omega_2 G_{\rm L}(\omega_2)\langle\mathbb{B}\mathbb{D}\rangle + \omega_2 G_{\rm L}(-\omega_2)\langle\mathbb{A}\mathbb{C}\rangle], \tag{D4}$$

$$\mathcal{J}_{\rm R} = \tfrac{1}{2}\Omega\cos^2\theta[G_{\rm R}(-\Omega)\langle\mathbb{C}\rangle - G_{\rm R}(\Omega)\langle\mathbb{D}\rangle]. \tag{D5}$$

Substitution of the transformed operators relation given in Eq. (A8) to Eq. (D5) yields the heat current relation in terms of bare operators and given in Eq. (7). Even though Eqs. (D1)–(D5) are easy to solve, the analytical expressions are too cumbersome to report, but we have confirmed that $\mathcal{J}_{\rm L} + \mathcal{J}_{\rm R} = 0$ at the steady state.

[1] F. Giazotto, T. T. Heikkilä, A. Luukanen, A. M. Savin, and J. P. Pekola, Opportunities for mesoscopics in thermometry and refrigeration: Physics and applications, Rev. Mod. Phys. **78**, 217 (2006).

[2] N. A. Roberts and D. G. Walker, A review of thermal rectification observations and models in solid materials, Int. J. Therm. Sci. **50**, 648 (2011).

[3] N. Li, J. Ren, L. Wang, G. Zhang, P. Hanggi, and B. Li, Colloquium: Phononics: Manipulating heat flow with electronic analogs and beyond, Rev. Mod. Phys. **84**, 1045 (2012).

[4] G. Benenti, G. Casati, K. Saito, and R. S. Whitney, Fundamental aspects of steady-state conversion of heat to work at the nanoscale, Phys. Rep. **694**, 1 (2017).

[5] M. Terraneo, M. Peyrard, and G. Casati, Controlling the Energy Flow in Nonlinear Lattices: A Model for a Thermal Rectifier, Phys. Rev. Lett. **88**, 094302 (2002).

[6] B. Li, L. Wang, and G. Casati, Thermal Diode: Rectification of Heat Flux, Phys. Rev. Lett. **93**, 184301 (2004).

[7] J. Lan and B. Li, Thermal rectifying effect in two- dimensional anharmonic lattices, Phys. Rev. B **74**, 214305 (2006).

[8] J. Lan and B. Li, Vibrational spectra and thermal rectification in three-dimensional anharmonic lattices, Phys. Rev. B **75**, 214302 (2007).

[9] N. Yang, N. Li, L. Wang, and B. Li, Thermal rectification and negative differential thermal resistance in lattices with mass gradient, Phys. Rev. B **76**, 020301(R) (2007).

[10] W. C. Lo, L. Wang, and B. Li, Thermal transistor: Heat flux switching and modulating, J. Phys. Soc. Jpn. **77**, 054402 (2008).

[11] C. W. Chang, D. Okawa, A. Majumdar, and A. Zettl, Solid-state thermal rectifier, Science **314**, 1121 (2006).

[12] B. Li, L. Wang, and G. Casati, Negative differential thermal resistance and thermal transistor, Appl. Phys. Lett. **88**, 143501 (2006).

[13] J. Hwang, M. Pototschnig, R. Lettow, G. Zumofen, A. Renn, S. Götzinger, and V. Sandoghdar, A single-molecule optical transistor, Nature (London) **460**, 76 (2009).

[14] J. Ordonez-Miranda, Y. Ezzahri, J. Drevillon, and K. Joulain, Transistorlike Device for Heating and Cooling Based on the Thermal Hysteresis of vo_2, Phys. Rev. Appl. **6**, 054003 (2016).

[15] Y. Shen, M. Bradford, and J.-T. Shen, Single-Photon Diode by Exploiting the Photon Polarization in a Waveguide, Phys. Rev. Lett. **107**, 173902 (2011).

[16] B. Karimi, J. P. Pekola, M. Campisi, and R. Fazio, Coupled qubits as a quantum heat switch, Quantum Sci. Technol. **2**, 044007 (2017).

[17] A. Ronzani, B. Karimi, J. Senior, Y.-C. Chang, J. T. Peltonen, C.D. Chen, and J. P. Pekola, Tunable photonic heat transport in a quantum heat valve, Nat. Phys. **14**, 991 (2018).

[18] S. Barzanjeh, M. Aquilina, and A. Xuereb, Manipulating the Flow of Thermal Noise in Quantum Devices, Phys. Rev. Lett. **120**, 060601 (2018).

[19] T. Ojanen and A.-P. Jauho, Mesoscopic Photon Heat Transistor, Phys. Rev. Lett. **100**, 155902 (2008).

[20] K. Joulain, J. Drevillon, Y. Ezzahri, and J. Ordonez-Miranda, Quantum Thermal Transistor, Phys. Rev. Lett. **116**, 200601 (2016).

[21] G. T. Landi, E. Novais, M. J. de Oliveira, and D. Karevski, Flux rectification in the quantum *XXZ* chain, Phys. Rev. E **90**, 042142 (2014).

[22] T. Werlang, M. A. Marchiori, M. F. Cornelio, and D. Valente, Optimal rectification in the ultrastrong coupling regime, Phys. Rev. E **89**, 062109 (2014).
[23] Z.-X. Man, N. B. An, and Y.-J. Xia, Controlling heat flows among three reservoirs asymmetrically coupled to two two-level systems, Phys. Rev. E **94**, 042135 (2016).
[24] J. Ordonez-Miranda, Y. Ezahri, and K. Joulain, Quantum thermal diode based on two interacting spinlike systems under different excitations, Phys. Rev. E **95**, 022128 (2017).
[25] B. Roche, P. Roulleau, T. Jullien, Y. Jompol, I. Farrer, D. A. Ritchie, and D. C. Glattli, Harvesting dissipated energy with a mesoscopic ratchet, Nat. Commun. **6**, 6738 (2015).
[26] H. Thierschmann, R. Sánchez, B. Sothmann, F. Arnold, C. Heyn, W. Hansen, H. Buhmann, and L. W. Molenkamp, Three-terminal energy harvester with coupled quantum dots, Nat. Nanotechnol. **10**, 854 (2015).
[27] L. Wang and B. Li, Thermal Logic Gates: Computation with Phonons, Phys. Rev. Lett. **99**, 177208 (2007).
[28] P. Pfeffer, F. Hartmann, S. Hofling, M. Kamp, and L. Worschech, Logical Stochastic Resonance with a Coulomb-Coupled Quantum-Dot Rectifier, Phys. Rev. Appl. **4**, 014011 (2015).
[29] J. Roßnagel, S. T. Dawkins, K. N. Tolazzi, O. Abah, E. Lutz, F. Schmidt-Kaler, and K. Singer, A single-atom heat engine, Science **352**, 325 (2016).
[30] B. Karimi and J. P. Pekola, Otto refrigerator based on a superconducting qubit: Classical and quantum performance, Phys. Rev. B **94**, 184503 (2016).
[31] L. P. Kouwenhoven, A. T. Johnson, N. C. van der Vaart, C. J. P. M. Harmans, and C. T. Foxon, Quantized Current in a Quantum-Dot Turnstile using Oscillating Tunnel Barriers, Phys. Rev. Lett. **67**, 1626 (1991).
[32] V. Moldoveanu, V. Gudmundsson, and A. Manolescu, Nonadiabatic transport in a quantum dot turnstile, Phys. Rev. B **76**, 165308 (2007).
[33] V. Gudmundsson, O. Jonasson, C.-S. Tang, H.-S. Goan, and A. Manolescu, Time-dependent transport of electrons through a photon cavity, Phys. Rev. B **85**, 075306 (2012).
[34] P. Reimann, M. Grifoni, and P. Hänggi, Quantum Ratchets, Phys. Rev. Lett. **79**, 10 (1997).
[35] G. Casati and C. Mejia-Monasterio, Heat flow in classical and quantum systems and thermal rectification, AIP Conf. Proc. **965**, 221 (2007).
[36] V. Balachandran, G. Benenti, E. Pereira, G. Casati, and D. Poletti, Heat current rectification in segmented *XXZ* chains, Phys. Rev. E **99**, 032136 (2019).
[37] C. Dames, Solid-state thermal rectification with existing bulk materials, J. Heat Transfer **131**, 061301 (2009).
[38] A. A. Maznev, A. G. Every, and O. B. Wright, Reciprocity in reflection and transmission: What is a 'phonon diode'? Wave Motion **50**, 776 (2013).
[39] A. Jeżowski and J. Rafalowicz, Heat flow asymmetry on a junction of quartz with graphite, Phys. Status Solidi A **47**, 229 (1978).
[40] D. D. Bhaktavatsala Rao and G. Kurizki, From Zeno to anti-Zeno regime: Decoherence-control dependence on the quantum statistics of the bath, Phys. Rev. A **83**, 032105 (2011).
[41] T. Moriya, Anisotropic superexchange interaction and weak ferromagnetism, Phys. Rev. **120**, 91 (1960).
[42] I. Dzyaloshinsky, A thermodynamic theory of weak ferromagnetism of antiferromagnetics, J. Phys. Chem. Solids **4**, 241 (1958).
[43] I. S. Tupitsyn, N. V. Prokof'ev, and P. C. E. Stamp, Effective Hamiltonian in the problem of a "central spin" coupled to a spin environment, Int. J. Mod. Phys. B **11**, 2901 (1997).
[44] P. L. Knight, Quantum fluctuations and squeezing in the interaction of an atom with a single field mode, Phys. Sci. **1986**, 51 (1986).
[45] L. Schoendorff and H. Risken, Analytic solution of the density-operator equation for the Raman-coupled model with cavity damping, Phys. Rev. A **41**, 5147 (1990).
[46] S. J. D. Phoenix and P. L. Knight, Periodicity, phase, and entropy in models of two-photonresonance, J. Opt. Soc. Am. B **7**, 116 (1990).
[47] B. C. Travaglione and G. J. Milburn, Implementing the quantum random walk, Phys. Rev. A **65**, 032310 (2002).
[48] J. R. Johansson, G. Johansson, and F. Nori, Optomechanical-like coupling between superconducting resonators, Phys. Rev. A **90**, 053833 (2014).
[49] A. Blais, R.-S. Huang, A. Wallraff, S. M. Girvin, and R. J. Schoelkopf, Cavity quantum electrodynamics for superconducting electrical circuits: An architecture for quantum computation, Phys. Rev. A **69**, 062320 (2004).
[50] A. Blais, J. Gambetta, A. Wallraff, D. I. Schuster, S. M. Girvin, M. H. Devoret, and R. J. Schoelkopf, Quantum-information processing with circuit quantum electrodynamics, Phys. Rev. A **75**, 032329 (2007).
[51] S.-B. Zheng, C.-P. Yang, and F. Nori, Arbitrary control of coherent dynamics for distant qubits in a quantum network, Phys. Rev. A **82**, 042327 (2010).
[52] J. Bernád and J. M. Torres, Partly invariant steady state of two interacting open quantum systems, Phys. Rev. A **92**, 062114 (2015).
[53] C. K. Law, Effective Hamiltonian for the radiation in a cavity with a moving mirror and a time-varying dielectric medium, Phys. Rev. A **49**, 433 (1994).
[54] C. K. Law, Interaction between a moving mirror and radiation pressure: A Hamiltonian formulation, Phys. Rev. A **51**, 2537 (1995).
[55] J. K. Moqadam, R. Portugal, and M. C. de Oliveira, Quantum walks on a circle with optomechanical systems, Quant. Info. Proc. **14**, 3595 (2015).
[56] H. P. Breuer and F. Petruccione, *The Theory of Open Quantum Systems* (Oxford University Press, Oxford, 2002).
[57] A. Rivas, A. Douglas K. Plato, S. F. Huelga, and M. B. Plenio, Markovian master equations: A critical study, New J. Phys. **12**, 113032 (2010).
[58] P. P. Hofer, M. P. Llobet, D. M. Miranda, G. Haack, R. Silva, J. B. Brask, and N. Brunner, Markovian master equations for quantum thermal machines: Local versus global approach, New J. Phys. **19**, 123037 (2017).
[59] A. Levy and R. Kosloff, The local approach to quantum transport may violate the second law of thermodynamics, EPL **107**, 20004 (2014).
[60] P. D. Manrique, F. Rodríguez, L. Quiroga, and N. F. Johnson, Nonequilibrium quantum systems: Divergence between global and local descriptions, Adv. Condens. Matter Phys. **2015**, 615727 (2015).

[61] J. O. González, L. A. Correa, G. Nocerino, J. P. Palao, D. Alonso, and G. Adesso, Testing the validity of the 'local' and 'global' GKLS master equations on an exactly solvable model, Open Syst. Inf. Dyn. **24**, 1740010 (2017).

[62] R. Alicki and R. Kosloff, Introduction to quantum thermodynamics: History and prospects, arXiv:1801.08314 (2018).

[63] J. R. Johansson, P. D. Nation, and F. Nori, QuTiP 2: A Python framework for the dynamics of open quantum systems, Comput. Phys. Commun. **184**, 1234 (2013).

[64] C. M. Pontes Carneiro and G. Queiroz Pellegrino, Application of an inverse Holstein-Primakoff transformation to the Jaynes-Cummings model, arXiv:1712.07589 (2017).

[65] G. Lindblad, On the generators of quantum dynamical semigroups, Commun. Math. Phys. **48**, 119 (1976).

[66] V. Gorini, A. Kossakowski, and E. C. G. Sudarshan, Completely positive dynamical semigroups of *N*-level systems,, J. Math. Phys. **17**, 821 (1976).

[67] G. Gordon and G. Kurizki, Preventing Multipartite Disentanglement by Local Modulations, Phys. Rev. Lett. **97**, 110503 (2006).

[68] G. Gordon and G. Kurizki, Scalability of decoherence control in entangled systems, Phys. Rev. A **83**, 032321 (2011).